


Carrier density and light helicity dependence of photocurrent in mono- and bilayer graphene

X Qian^{1,4}, B Cao^{2,4}, Z Wang^{2,3}, X Shen², C Soci^{2,3}, M Eginligil^{1,5}  and T Yu^{2,5}

¹Key Laboratory of Flexible Electronics (KLOFE) and Institute of Advanced Materials (IAM), Jiangsu National Synergetic Innovation Center for Advanced Materials (SICAM), Nanjing Tech University (NanjingTech), 30 South Puzhu Road, Nanjing 211816, People's Republic of China

²Division of Physics and Applied Physics, School of Physical and Mathematical Sciences, Nanyang Technological University, Singapore, 637371

³Centre for Disruptive Photonic Technologies, Nanyang Technological University, 21 Nanyang Link, Singapore 637371

E-mail: yuting@ntu.edu.sg and iameginligil@njtech.edu.cn

Received 13 April 2018, revised 2 September 2018

Accepted for publication 20 September 2018

Published 15 October 2018



CrossMark

Abstract

Helicity-dependent photocurrent in monolayer graphene has been the subject of intense debate, and was recently ascribed to photon drag and circular photogalvanic effects. Unlike inversion symmetric monolayer graphene with no band gap, the most stable case of two-layer graphene, AB-stacked bilayer graphene, has broken inversion symmetry and can have a band gap upon electrical gating. Here we report the experimental determination of the photocurrent response of mono- and bilayer graphene as a function of light polarization, as well as carrier density and polarity. The mono- and bilayer graphene data show qualitative features in common with the photocurrent contribution that is expected to arise from the photon drag effect. On the other hand, the photocurrent due to the circular photogalvanic effect in bilayer (monolayer) graphene has asymmetric (symmetric) dependence on carrier density, which is attributed to particle-hole asymmetry.

Keywords: condensed matter (graphene), materials science, nanophysics, optoelectronics

(Some figures may appear in colour only in the online journal)

1. Introduction

Research in graphene optoelectronics is one of the fastest developing platforms for studying light–matter interaction [1]. Beyond the active research into the new fundamental aspects of this and related systems [2], the unique optical and electronic properties of graphene can be employed in numerous applications, such as highly sensitive bolometers [3], photodetectors, plasmonic or photovoltaic devices [4, 5], which leverage photo-induced thermal and electronic effects. The characteristics of photocurrent (PC) in graphene have been extensively studied, resorting to different types of

devices and configurations, such as p-n junctions [6–8] or metal/graphene interfaces [9]. By tuning light frequency and pulse widths in addition to varying source–drain and gate voltages, it is possible to distinguish the thermoelectric, photovoltaic, and bolometric effects in the observed photo-conductivity [10]. The state of polarization adds another dimension to the parameter space available to control the PC; understanding its effect and how to harness its consequences is crucial for photonic device concepts.

The non-linear DC electrical response of electrons to the light field can be generically written, to second order, as

$$j_{\alpha}(q=0) = S_{\alpha\beta\gamma} \frac{E_{\beta}E_{\gamma}^{*} + E_{\beta}^{*}E_{\gamma}}{2} + A_{\alpha\beta\gamma} \frac{E_{\beta}E_{\gamma}^{*} - E_{\beta}^{*}E_{\gamma}}{2}, \quad (1a)$$

⁴ Equal contributors.

⁵ Authors to whom any correspondence should be addressed.

$$j_{\alpha}(q \neq 0) = S_{\alpha\beta\gamma\nu} q_{\beta} \frac{E_{\gamma} E_{\nu}^* + E_{\gamma}^* E_{\nu}}{2} + A_{\alpha\beta\gamma\nu} q_{\beta} \frac{E_{\gamma} E_{\nu}^* - E_{\gamma}^* E_{\nu}}{2}, \quad (1b)$$

where $S_{\alpha\beta\gamma}$ ($S_{\alpha\beta\gamma\nu}$) and $A_{\alpha\beta\gamma}$ ($A_{\alpha\beta\gamma\nu}$) are symmetric and anti-symmetric tensors of rank three (four) [11]. Here \mathbf{q} is the momentum of light and equations (1a) and (1b) describe cases without and with transfer of momentum from incident photons to excited carriers, respectively. The splitting of the quadratic response as symmetric and antisymmetric is advantageous because (i) the anti-symmetric combination of fields in the second term is directly proportional to the degree of circular polarization of the incoming light, and (ii) the symmetric and anti-symmetric character of these tensors assists in identifying which terms survive for a given point symmetry of the target system. This current is strongly dependent on the polarization and orientation of the incoming radiation, and effects such as the photogalvanic effect (PGE) and the photon drag effect (PDE), are intrinsically associated with specific polarization states [12] (for example, the so-called linear PDE, circular PDE, linear PGE, and circular PGE). The motivation for making this distinction among the various contributions to the PC explicitly lies in the distinct signatures that they display, namely a symmetry/anti-symmetry with the inversion of helicity for linear and circular contributions to PC, respectively. Whether such quadratic response terms are permitted is determined microscopically by the dependence of the allowed optical transitions on the polarization, as well as by symmetry constraints that require, foremost, the absence or breaking of inversion symmetry, and as well as other constraints imposed by the 6-fold (3-fold) and horizontal plane symmetries of monolayer graphene (bilayer graphene). For inversion symmetric monolayer graphene (bilayer graphene—broken inversion symmetry) the point symmetry is D_{6h} (D_{3d}), which is reduced to C_{6v} (C_{3v}) when graphene is placed on a substrate. This behaviour can be probed by measuring the PC as a function of the polarization state (phase angle) of the incident light, which can be readily achieved by passing linearly polarized light through a quarter wave plate ($\lambda/4$ plate). The plate's optical axis with respect to the incoming linear polarization, φ , defines the helicity of the outgoing light, afterwards directed at the sample. Expressing the electric field amplitudes in equation (1) in terms of this quarter-wave plate angle φ , the PC j_{α} can be cast generically as

$$j_{\alpha} = (C_{1PGE} + C_{1PDE}) \sin 2\varphi + (L_{1PGE} + L_{1PDE}) \sin 4\varphi + (L_{2PGE} + L_{2PDE}) \cos 4\varphi + (D_{PGE} + D_{PDE} + D_{NP}). \quad (2)$$

This expression encodes the most general dependence of the PC on the polarization state arising from equation (1), and defines the so-called linear PGE (L_{1PGE} and L_{2PGE})—LPGE, linear PDE (L_{1PDE} and L_{2PDE})—LPDE, circular PGE (C_{1PGE})—CPGE, and circular PDE (C_{1PDE})—CPDE contributions to the PC. The last term in equation (1) has three components: the first two are due to PGE or PDE, D_{PGE} and D_{PDE} and the last one,

D_{NP} , arises from polarization-independent effects. All the polarization-dependent PC contributions in equation (2) can be given as follows: $C_{1PGE}(L_{1PGE}) = I f_{C_{1PGE}}(\theta, S_{\alpha\beta\gamma}, A_{\alpha\beta\gamma})$ ($f_{L_{1PGE}}(\theta, S_{\alpha\beta\gamma}, A_{\alpha\beta\gamma})$) and $C_{1PDE}(L_{1PDE}) = I f_{C_{1PDE}}(\theta, S_{\alpha\beta\gamma\nu}, A_{\alpha\beta\gamma\nu})$ ($f_{L_{1PDE}}(\theta, S_{\alpha\beta\gamma\nu}, A_{\alpha\beta\gamma\nu})$), where I is the light intensity (E^2). L_{2PGE} (L_{2PDE}) can be expressed similar to L_{1PGE} (L_{2PDE}).

Here, $f_{C_{1PGE}}(\theta, S_{\alpha\beta\gamma}, A_{\alpha\beta\gamma})$ ($f_{L_{1PGE}}(\theta, S_{\alpha\beta\gamma}, A_{\alpha\beta\gamma})$) and $f_{C_{1PDE}}(\theta, S_{\alpha\beta\gamma\nu}, A_{\alpha\beta\gamma\nu})$ ($f_{L_{1PDE}}(\theta, S_{\alpha\beta\gamma\nu}, A_{\alpha\beta\gamma\nu})$) are the functions with angle of incidence θ (this partly comes from the electric field unit vector direction depending on the transmission coefficients for linear polarization based on Fresnel's formula [11]) and the tensor components of $S_{\alpha\beta\gamma}$ and $A_{\alpha\beta\gamma}$ ($S_{\alpha\beta\gamma\nu}$ and $A_{\alpha\beta\gamma\nu}$) dependencies for the CPGE (LPGE) and the CPDE (LPDE) currents. All these are a purely geometric consequence of equation (1) and, hence, hold independently of the microscopic details at play determining the PC components. These can be readily identified through their different periodicity on the angle φ , and the explicit functions based on the incidence angles and tensor components are omitted for ease of notation. For longitudinal PC—where the incidence plane is parallel to the current direction—all C_1 terms and all L_1 terms are negligible and all L_2 and all D are the major components; for transverse PC—where the incidence plane is perpendicular to the current direction—all L_2 and all D are negligible and all C_1 and all L_1 are the major components. The absence (presence) of C_1 in longitudinal (transverse) PC is in agreement with the expectation from the phenomenology, which is based on the geometry of impinging light with the polarized state and point symmetry.

At energies near the charge neutrality point (CNP), the elementary electronic excitations in an atomically thin monolayer graphene (1LG) behave as massless Dirac fermions, characterized by a Berry phase of π as observed in the anomalous quantum Hall effect [13]. The absence of a band gap in the electronic spectrum of 1LG limits its direct utilization in many electronic applications that rely on the semi-conducting characteristics of the underlying material. This limitation can be overcome, in principle, with 2LG since a band gap can be opened and tuned by driving a potential difference between the two layers [14–16]. This electrostatic breaking of the layer symmetry can be achieved with chemical doping [17], a direct utilisation of independent top and bottom gates [18–21], or a combination of both [16], and thus a continuously tunable bandgap of up to 250 meV can be obtained. Electrons in 2LG have intrinsically different properties than 1LG, such as the different energy–momentum relation, $E_p = p^2/2m$ with effective mass m , different chirality, and a different Berry phase of 2π [22, 23].

In this work, we experimentally identify the conventional contributions to the PC that are due to the linear and circular components of light impinging on a globally back-gated 1LG and 2LG. We distinguish these contributions from their characteristic dependence on the polarization state, and characterize their sensitivity to the carrier density that can be varied by the field effect. The PC contributions are symmetric

with respect to the time-reversal change sign at the CNP for both 1LG and 2LG, as expected. However, for 2LG, our measurement results are seen to be best fitted with the inclusion of an additional term which has $\cos \varphi$ dependence, which cannot be explained in terms of quadratic response theory up to second order.

2. Materials and methods

Monolayer and bilayer graphene flakes were prepared by mechanical cleavage from highly ordered pyrolytic graphite and transferred onto a SiO_2 (300 nm)/Si wafer. The 300 nm thickness of the oxide enhanced the visual contrast in order to locate the graphene through an optical microscope and to estimate its layer number. Graphene thicknesses were confirmed by Raman measurements. The flakes were then processed into devices by standard e-beam lithography techniques and deposition of Ti (5 nm)/Au (75 nm) contacts for electrical and PC measurements.

The PC is measured at room temperature by the illumination of graphene and bilayer graphene devices under a continuous wave laser with $\hbar\omega = 2.33$ eV and a focus spot 200 μm wide. A schematic diagram of the setup is given in figure 1(a). The linearly polarized laser beam is chopped at a frequency of 137 Hz before passing through a $\lambda/4$ retarder, and is subsequently directed obliquely (incidence angle θ) towards the sample in such a way as to keep the spot center aligned with the geometrical center of the sample. The PC at the chopping frequency is measured with a lock-in amplifier. This experimental setup allows one to continuously vary the helicity of the radiation reaching the device by rotating the wave plate, and we use the angle φ between the plate's fast axis and the initial linear polarization as the parameter that identifies a particular helicity.

Light impinges on the sample at a constant $\theta = 50^\circ$ oblique incidence and the current is measured perpendicularly to the plane of incidence. An electric field is applied perpendicularly via a global back-gate provided by the doped-Si portion of the substrate, which allows variation of the carrier density by the field effect. The sample preparation was done as described previously elsewhere [24]. The AB stacking of the 2LG sample as well as the layer thickness of 1LG and 2LG were confirmed by Raman spectroscopy [25]. Figures 1(b) and (c) show that the measured PC varies linearly with laser intensity, for 1LG and 2LG, respectively. This linear dependence of the photocurrent arises from the quadratic response to the electromagnetic field. All the measurements discussed below are performed at a constant intensity of 8 W cm^{-2} .

3. Results and discussion

We want to emphasize that where our work differs from previous light helicity-dependent photocurrent studies of graphene is the photon energy of 2.33 eV that we use, unlike the previous body of work focused on terahertz frequencies,

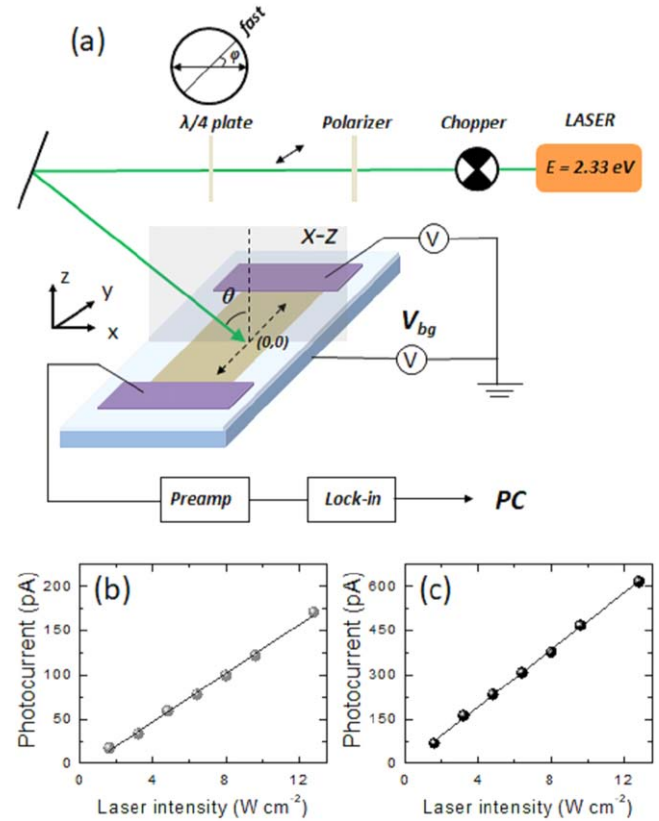


Figure 1. The photocurrent setup and photocurrent of the graphene samples. In (a), we schematically depict the measurement layout. The centre of the graphene devices with Ti/Au electrodes defines the origin ($y = 0, x = 0$) of the coordinates in the plane. The laser frequency is $\hbar\omega = 2.33$ eV. Characterization of the photocurrent as a function of laser intensity (points), and the best linear fit (line) for monolayer graphene (b) and bilayer graphene (c) are shown. Polarization-dependence studies were performed at 8 W cm^{-2} .

with energies less than 200 meV [26–32]. Particularly in the far infrared range of 10–20 meV, the CPDE term becomes more important than the CPGE term [27, 28]. However the CPDE term is suppressed in our measurements. Also, both 1LG and 2LG are centrosymmetric, which means that the LPGE and D_{PGE} are not expected. Therefore, we only consider $C_{1\text{PGE}}, L_{1\text{PDE}}, L_{2\text{PDE}}, D_{\text{PDE}}$ and D_{NP} . Since D_{PDE} contains an L_2 related contribution, from now on for simplicity we label $C_{1\text{PGE}}$ as C_1 , $L_{1\text{PDE}}$ as L_1 , $L_{2\text{PDE}} + D_{\text{PDE}}$ as L_2 , and D_{NP} as D . Then we can re-write equation (2) as

$$j_\alpha = C_1 \sin 2\varphi + L_1 \sin 4\varphi + L_2 \cos 4\varphi + D. \quad (3)$$

The photocurrent of 1LG and 2LG devices are measured as depicted in figures 2(a)–(d), respectively. The PC data are plotted in the transverse (perpendicular to the incidence plane) and longitudinal (parallel to the incidence plane) geometries, as shown in the inset of figures 2(a), (c) and (b), (d), respectively. The PC data points represented by black circles can be fitted by the phenomenological formula expressed by equation (3), where C_1 is the PC component associated with the circular component of the incoming light, L_1 and L_2 with the linear components, and D represents the polarization-independent terms. The PC magnitude is in the sub nano-ampere range, and L_2 and D are about

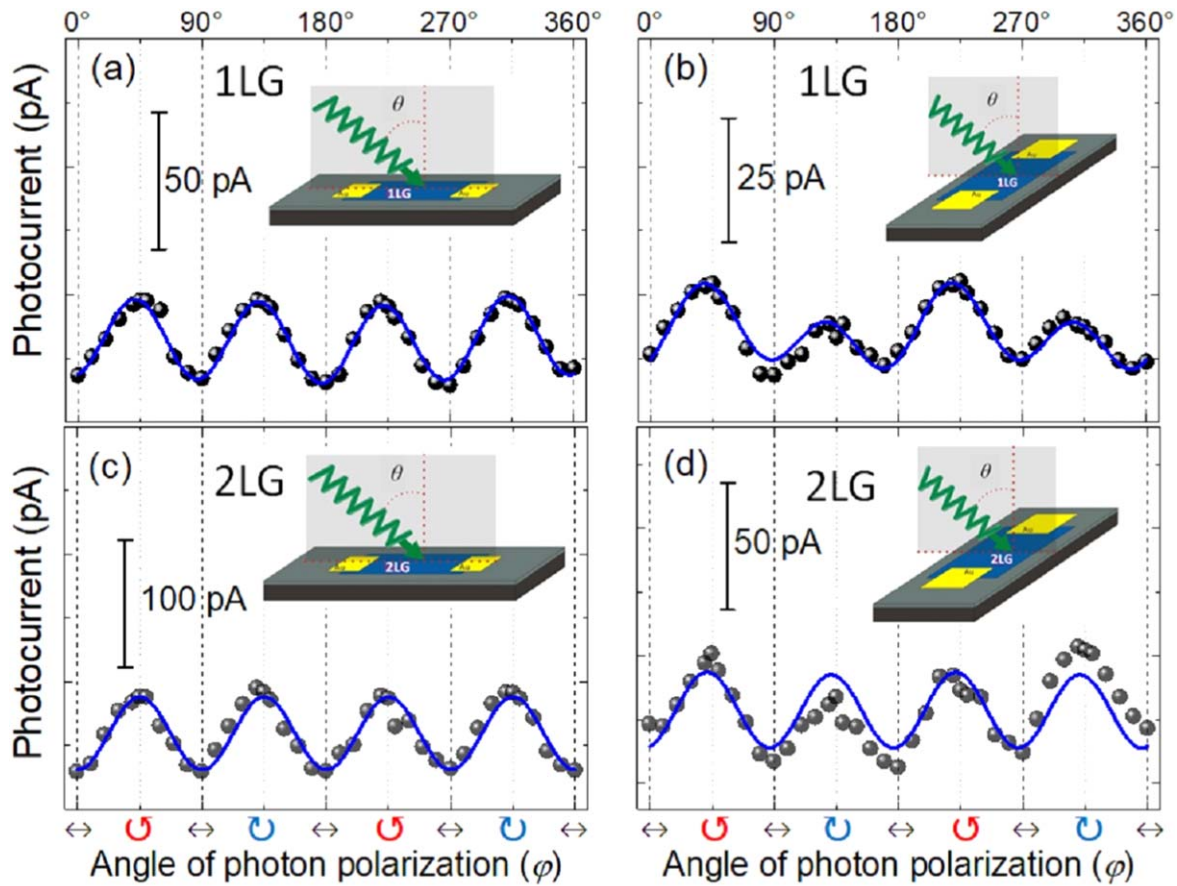


Figure 2. Photocurrent as a function of the angle of the quarter-wave plate, φ , for monolayer graphene (a), (b) and bilayer graphene (c), (d). The data are acquired at fixed oblique incidence ($\theta = 50^\circ$) with two different azimuthal alignments; namely, (a)–(c) and (b)–(d) show the data for azimuthal alignment with the plane of incidence parallel to the Oyz and Oxz planes, respectively, as shown in the insets. All data represented by the black circles and blue solid curves are the fits to equation (3) to extract phenomenological photocurrent constants, such as C_1 , L_1 , L_2 , D . In longitudinal geometry, the adjacent R-square values of the fitting in 1LG (a) and in 2LG (c) are 0.97 and 0.96, respectively. In transverse geometry, the adjacent R-square values of the fitting in 1LG (b) and in 2LG (d) are 0.93 and 0.64, respectively.

15 (30) pA and 110 (260) pA for 1LG (2LG), respectively. In 1LG (2LG), the magnitude of the transverse PC components C_1 , L_2 , and D are 2.5 (1.5) pA, 8 (15) pA, 105 (280) pA, respectively.

The fitting curve for 1LG in transverse geometry has an adjacent R-square (the value which indicates the compatibility of the fitting) of 0.93 (figure 2(b)). However, this value is 0.64 for 2LG, as seen in figure 2(d), implying that this fitting is not good and requires further attention. In fact, there is a clear deviation of the black data points from the blue curve, particularly at linearly (\leftrightarrow) polarized states $\varphi = 0^\circ$, 90° , 180° , and 270° and at circularly polarized states $\varphi = 45^\circ$ (left-circularly polarized light, \ominus), $\varphi = 135^\circ$ (right-circularly polarized light, \odot), $\varphi = 225^\circ$ (\ominus), and $\varphi = 315^\circ$ (\odot).

To study this sensitivity of the PC to the character and density of the charge carriers, the same measurements are repeated at different back-gate voltages (V_{bg}). Figures 3(a) and (c) present the resistance as a function of the V_{bg} characteristic of 1LG and 2LG, which is hole-doped at zero V_{bg} and has a CNP at around 20 and 32 V, respectively, where the resistance reaches its maximum value. The corresponding back-gate-dependent PC signals measured at $\varphi = 0^\circ$ are shown in figures 3(b) and (d): they are characterized by a

monotonic increase in magnitude from $V_{bg} \approx -50$ V to $V_{bg} \approx 5$ V (in this range the PC increases by 50 pA and 100 pA for 1LG and 2LG, respectively), followed by a fast decrease in magnitude and sign change at the CNP associated with the transition from hole to electron conduction. The gate voltage corresponding to zero PC coincides with the CNP extracted from the resistance characteristic. In the electron conduction regime, the PC slowly increases and saturates around 120 pA at $V_{bg} = 50$ V for 1LG, while a slow increase continues for 2LG, from their respective CNP. Unlike the symmetric behaviour of the PC magnitude versus back-gate voltage for 1LG with respect to the CNP, there is a noticeable asymmetry around CNP for 2LG. This large asymmetry arises from the polarization-independent term of the PC, as explained later.

With the ability to vary the back-gate voltage, the PC components C_1 and L_2 can be studied as a function of carrier sign and density, n . We carried out such a study by extracting the transverse PC $j_y(n, \varphi)$ in the full range of φ and fitting to equation (3) for each density. In figures 4(a), (b) (figures 4(c), (d)), the CPGE current C_1 (the LPDE current L_2) as a function of selected V_{bg} s are plotted for 1LG and 2LG, respectively.

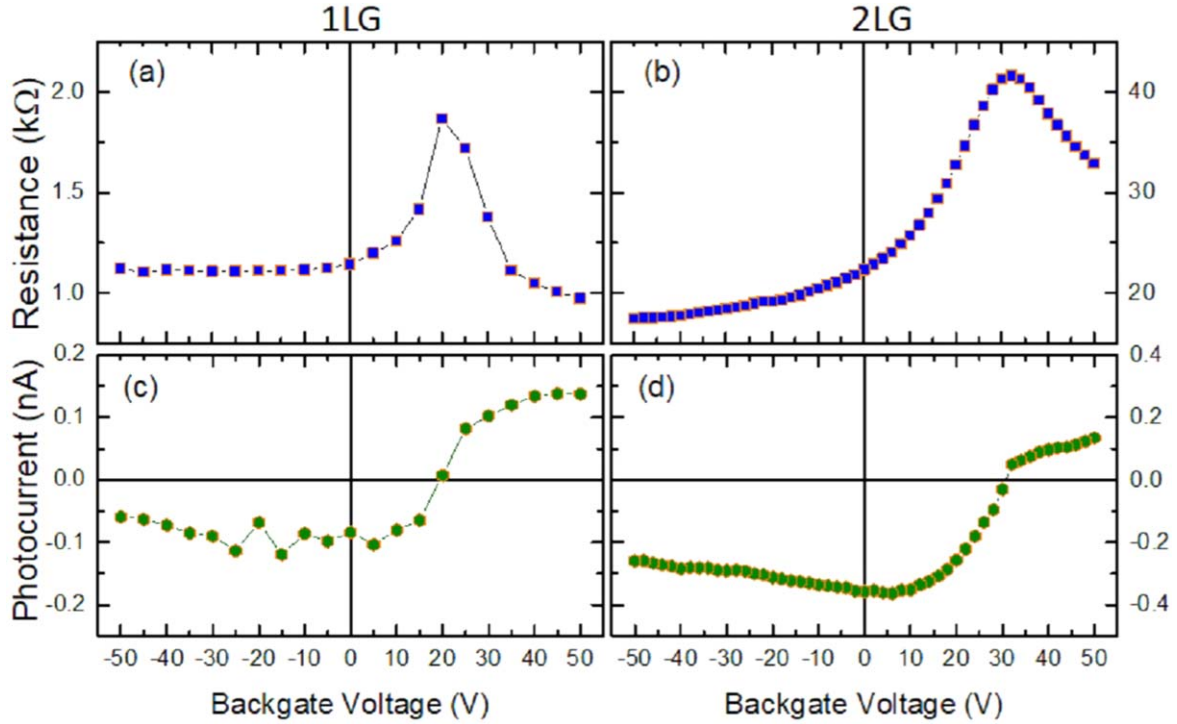


Figure 3. Dependence of the resistance and the photocurrent on the back-gate voltage for graphene and bilayer graphene samples at $\varphi = 0^\circ$. The resistance versus back-gate voltage of graphene (1LG) (a) and bilayer graphene (2LG) (b) are given. (c) and (d) represent the photocurrent magnitude at a given back-gate voltage, for 1LG and 2LG, respectively. The charge neutrality point is identified by the peak in the resistance circa 20 V and 32 V for 1LG and 2LG. This coincides with the voltage at which the photocurrent changes sign as a result of the modification of carrier type.

The fitting curves are the Fermi–Dirac functions and the physical interpretation can be understood as follows. At the microscopic level, the LPDE current can be characterized on general grounds in terms of the transition rate $M_{b,a}^q$ from an initial electronic state a to a final state b of the electron due to illumination with photons having wave vector q and simultaneous scattering by impurities or phonons. The second-order DC response can be written as [11]

$$j_{\text{LPDE}} = \frac{8\pi e}{\hbar} \sum_{a,b} [\nu_b \tau(\varepsilon_b) - \nu_a \tau(\varepsilon_a)] |M_{b,a}^q|^2 \times [f(\varepsilon_a) - f(\varepsilon_b)] \delta(\varepsilon_b - \varepsilon_a - \hbar\omega), \quad (4)$$

where ν is the magnitude of the electron velocity, $\tau(\varepsilon)$ the momentum relaxation time, and $f(\varepsilon)$ the Fermi–Dirac distribution function. In figures 4(c) and (d), we observe a step-like behaviour of the PC with respect to V_{bg} , i.e. with respect to the chemical potential of the device. For both 1LG and 2LG, L_2 exhibits a similar symmetric behaviour near the CNP, as seen in figures 4(c), (d). The L_2 fits well to a Fermi–Dirac function (the dashed curve), which shows saturation, on negative values of PC, at 10 (27) V and, on positive values of PC, at 30 (37) V for 1LG (2LG). For 1LG, the PC component L_2 symmetrically saturates at -10 pA and 10 pA (figure 4(c)), and D saturates at -100 pA and 100 pA (figure 4(e)). For 2LG, the PC component L_2 symmetrically saturates at -15 pA and 15 pA (figure 4(d)), while the polarization-independent PC component D has an offset in the fitting function and does not symmetrically saturate. It saturates at -300 pA under hole doping, as seen in figure 4(f), and is

similar to the total PC amplitude behaviour previously shown in figure 3(d). Under electron doping, D seems to saturate at 100 pA, although we cannot be definitive with regards to the behaviour here given that the CNP is relatively close to our operational maximum positive back-gate voltages. This asymmetry with respect to the CNP in the saturation values of PC for the PC component D strengthens the hypothesis of graphene–substrate interaction, while the symmetry seen in the saturation of L_2 in the hole- and electron-doped regimes is consistent with the associated PC contribution arising from the PC due to light momentum transfer to the sample alone, which is related to particle-hole symmetry [27]. Indeed, the D term is polarization independent and its nature is quite different from L_2 , as is reflected in the saturation of the gate dependencies of L_2 and D . From the values of L_2 and D deep in the electron and hole-doped regimes, we estimate that $D/L_2 \sim 20$ and 6 in the p-type and n-type 2LG sample, respectively, while this value is ~ 10 in both the p-type and n-type 1LG sample.

For the excitation energies used in our experiments and the proximity to the CNP, we expect the PC to be dominated by electronic processes in the vicinity of the K and $-K$ points (or valleys) in the Brillouin zone. This is analogous to the spin-orientation-induced CPGE which takes place as a result of two different hole spin states in semiconductor quantum wells with C_s symmetry [11]. In the present case, instead of spin states, there are two different valleys, which lead to a modified optical transition matrix for electron wave vector k in the vicinity of $\pm K$, $M_{b,a}^{q=0}$, in equation (3). The PC

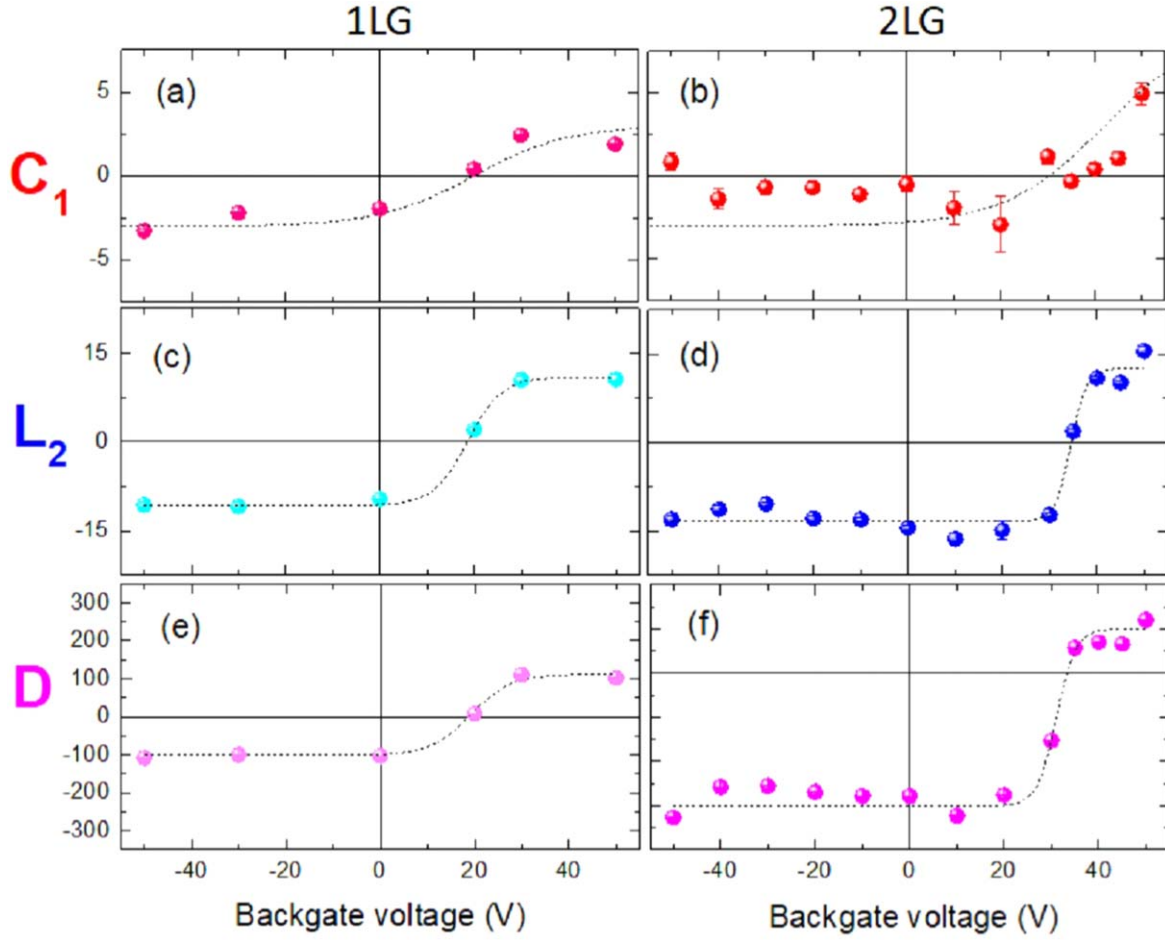


Figure 4. Photocurrent contribution, the CPGE current (C_1) and the LPDE current (L_2) as a function of back-gate voltage for circularly polarized light propagating in the Oxz plane for both monolayer graphene (1LG) and bilayer graphene (2LG) samples. Circles represent the numerical value obtained from the data fitting similar to the one described in figure 2 at each back-gate voltage. In panels (a), (b), the CPGE current (C_1) versus back-gate voltage for 1LG and 2G are given. In panels (c)–(d) the LPDE current (L_2) versus back-gate voltage for 1LG and 2G are given. In panels (e), (f) the polarization-independent current (D) versus back-gate voltage for 1LG and 2G are given. Error bars in the data points of C_1 , L_2 , and D are determined from phenomenological fitting at each back-gate voltage. The dashed lines are the Fermi–Dirac functions that best fit the data.

contribution due to the CPGE can then be expressed as [11]

$$j_{\text{CPGE}} = \frac{8\pi e}{\hbar} \sum_{a,b} [\nu_b \tau(\varepsilon_b) - \nu_a \tau(\varepsilon_a)] |M_{b,a}^{q=0}|^2 \times [f(\varepsilon_a) - f(\varepsilon_b)] \delta(\varepsilon_b - \varepsilon_a - \hbar\omega). \quad (5)$$

Without a detailed matrix analysis and a naive approach, $|M_{b,a}^{q=0}|^2$, which is due to direct interband transitions at the vicinity, is expected to be smaller than $|M_{b,a}^q|^2$, which is due to all transitions upon light momentum transfer. Therefore j_{CPGE} is expected to be smaller than j_{LPDE} . In figure 4(a), the C_1 term due to the CPGE is plotted as a function of V_{bg} for 1LG. The Fermi–Dirac fitting shows saturation on negative values of PC at -15 V and it is about to saturate on positive values of PC at the maximum V_{bg} . The PC component C_1 seems to symmetrically saturate at -3 pA and 3 pA. For the 2LG sample, the values fluctuate slightly for $V_{\text{bg}} < 20$ V, but there is an increasing trend from 20 V to 50 V and the fitting function has an offset. A comparison of (b) and (d) in this figure shows that C_1 is smaller than L_2 by a factor of ~ 5 in the hole-doped

regime, and by ~ 2 at the highest electron doping that we could achieve. The asymmetry in the V_{bg} dependence of the C_1 term can be due to processes influenced by electron–hole asymmetry [33], as observed in figure 3(d).

Note that, while the LPDE in 2LG could be similar to that in 1LG, the CPGE is expected to be much larger in 2LG. This is because the CPGE requires a component of the electric field normal to the graphene layer (\hat{z} direction), which is more efficient for 2LG, and for LPDE, the z -component of the electric field is in general not needed. However, there is no such pronounced enhancement of the CPGE in our data, which may be attributed to the low effective number of electrons per atom for polarization in the Oxy plane than for polarization in the \hat{z} direction [34], or to the high excitation energy used. Nevertheless, for both 1LG and 2LG, PCs arising from the CPGE can, in principle, be enhanced with the integration of tailored plasmonic structures, as the higher absorption that they promote should lead to a more pronounced PC response [35].

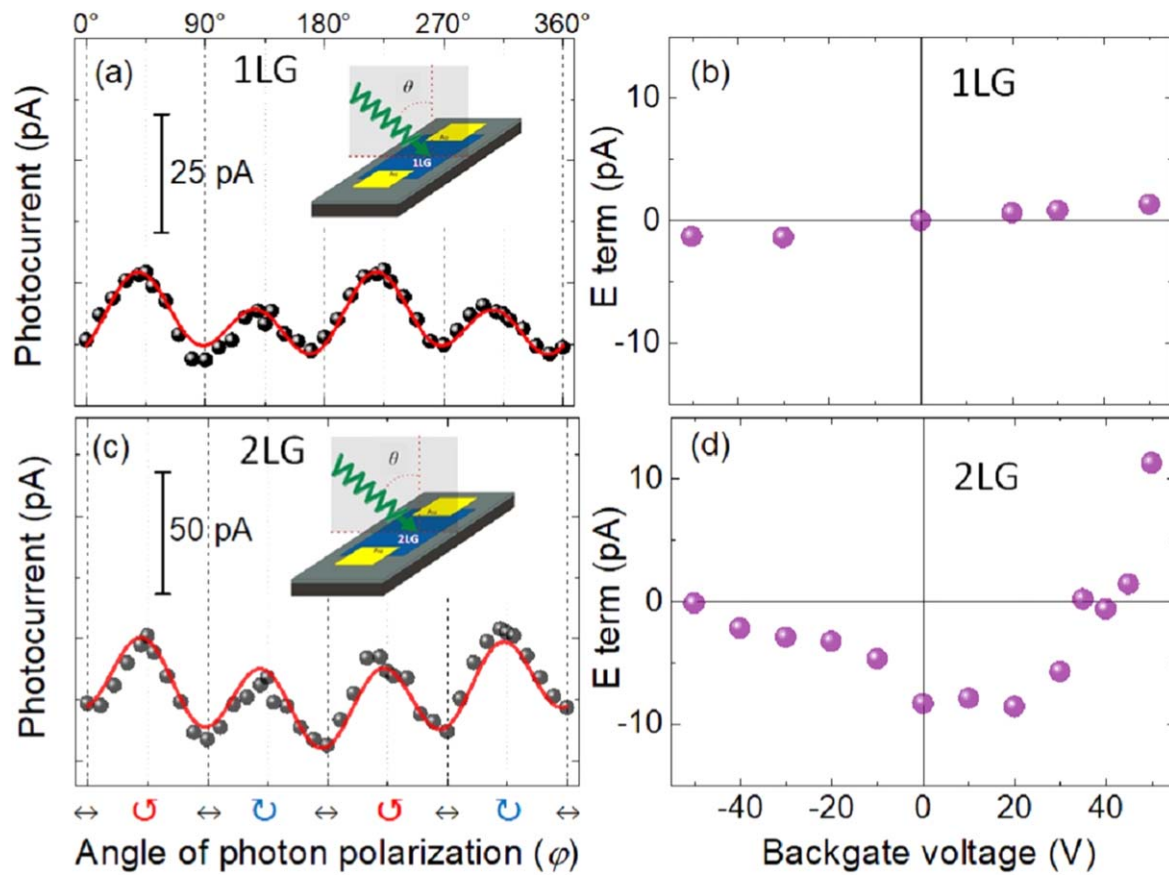


Figure 5. Photocurrent, at fixed oblique incidence ($\theta = 50^\circ$) and at zero gate voltage, as a function of the angle of photon polarization, φ , for monolayer graphene (a) and bilayer graphene (c), for azimuthal alignment with the plane of incidence parallel to the Oxz planes. All data are represented by black circles and the red solid curves are the fits to equation (3) with an additional $\cos \varphi$ dependent E term, to extract the additional contribution (E) in addition to the phenomenological photocurrent constants, such as C_1 , L_1 , L_2 , D . There is almost no difference between the fitting in (a) and the fitting in figure 2(b), which is reflected as a weak dependence of the E term versus back-gate voltage for monolayer graphene in (b). However, the fitting in (c) is a much better fitting (adjacent R-square = 0.86) than the fitting in figure 2(d) (adjacent R-square = 0.64). (d) A large variation of back-gate voltage dependence of the E term around the charge neutrality point (at ~ 32 V) in bilayer graphene is presented.

Another issue to be addressed is the deviation of data points from the fitting based on the phenomenological formula in figure 2(d) 2LG. The reason behind this could be due to imperfection in the optical setup, because, for $\varphi = 0^\circ$ and $\varphi = 180^\circ$, light must be linearly polarized with identical orientation of the electric field vector and thus the PC must have the same sign and amplitude, as is observed in 1LG. However, surprisingly, in 2LG, this is not the case. To see if we could get a better fitting of the experimental data, we include a new term, varying with $\cos \varphi$, into the phenomenological formula (equation (3)). Then, at $V_{bg} = 0$ V, we plot the transverse PC (i.e. perpendicular to the incidence plane) of both 1LG and 2LG in figures 5(a), (b) with the inclusion of $E \cos \varphi$ into equation (3), where E has pA units. Here, we need to emphasize that we are not defining a new phenomenological formula but just a new fitting function. Although there is almost no difference between the fittings in figures 2(b) and 5(a), for 1LG, the fitting of 2LG data with $E \cos \varphi$ in figure 5(c) is clearly much better than the fitting in figure 2(d), and the adjacent R-square is 0.86 with the new fitting. More interestingly, although the back-gate voltage

dependence of the E term in 1LG (figure 5(b)) is negligible, the E term varies non-monotonically with the back-gate voltage for the 2LG sample (figure 5(d)). Inspection of figure 5(d) shows that in the vicinity of the CNP ($10 \text{ V} < V_{bg} < 50 \text{ V}$) the E term is approximately linear in V_{bg} , and hence in carrier density, and is most pronounced at 10 V and 50 V. The E term is then progressively suppressed upon entering in the deep hole-doped regime, becoming zero at around -50 V. With the exception of the E term, the polarization dependence of the terms proportional to the PC contributions L_2 , C_1 , D follows directly from the DC response to an electromagnetic field in second order [11]. Although there is no existing phenomenology behind this, the fact that the inclusion of the E term clearly shows better fitting for 2LG while it does not make a clear difference for 1LG suggests that the deviation of the data points from the phenomenological fitting (equation (3)) is not simply due to imperfection in the optical setup.

In [26], the low-frequency (THz) PC response of monolayer graphene was studied, and its behaviour as a function of frequency, polarization and incidence angle has been attributed to the interplay between the so-called AC Hall

effect, a type of photon drag effect whereby momentum transfer occurs between the radiation field and the electrons and dominates at low frequency, and photogalvanic contributions that are possible if the substrate interaction is enough to break the inversion symmetry, and was seen to dominate at higher frequencies [26]. In contrast with the results reported in this study, where the PC is seen to be dominated by the contribution proportional to the light helicity ($\sim \sin 2\varphi Z$), our PC fits show that the current is dominated by the polarization-independent contribution in both geometries, followed by the linear term, and then CPGE in order of magnitude. From this perspective, qualitatively the PC response seen here in 1LG and 2LG shares similarity with that found in the three-dimensional topological insulator Bi_2Se_3 at high frequency [36] (in which the CPGE has a different physical origin, i.e. surface states), than the PC response of 1LG at low frequencies.

4. Conclusions

We studied the generation of a DC electrical current in monolayer graphene and bilayer graphene under illumination by a monochromatic laser field, with particular emphasis on its sensitivity upon the polarization state of the incoming light and the density and type of carriers in the system. The dependence on the polarization allowed us to identify different contributions to the PC: one due to LPDE, light momentum transfer to the sample, while the other one is due to CPGE. The PC contributions in transverse (longitudinal) geometry are those due to CPGE (LPDE). Based on the data and fittings to the phenomenological PC formula, the PC contributions due to the CPGE term, the LPDE term and the last term containing PGE, PDE, and polarization-independent parts are determined as a function of carrier densities for both mono- and bilayer graphene. The photocurrent due to LPDE is a symmetric PC contribution with regards to carrier type and with respect to the CNP for both mono- and bilayer graphene (as fitted by the Fermi-Dirac function), while the other two are from the CPGE and the combination of PGE, PDE, and polarization-independent contributions which seem to be still symmetric for monolayer graphene, unlike the case of bilayer graphene in which there is asymmetry due to the inherent particle-hole asymmetry. On the other hand, the angle of the photon polarization dependence of the PC and its fitting to the phenomenological PC formula has an adjacent R-square of 0.93 for monolayer graphene at zero gate voltage—this value is 0.64 for bilayer graphene. However, with the inclusion of a new term, varying with $\cos \varphi$, this value can be improved to 0.86 for bilayer graphene. Although there is no clear phenomenology and physical origin of this $\cos \varphi$ dependence in bilayer graphene, it is absent in monolayer graphene. Furthermore, a large variation of the carrier density dependence of this new term around the CNP in bilayer graphene is also observed. Thus, this warrants further experimental and theoretical investigation to identify

its prevalence across other electronic systems, and the underlying conditions and microscopic mechanism.

Acknowledgments

The authors are grateful to Prof. Vitor M Pereira and Dr Fabio Hipólito for fruitful discussions and useful suggestions. This work is supported in part by the Six Talent Peaks Project in Jiangsu Province under grant number 51235079, 100 Foreign Talents Project in Jiangsu Province under grant number 51235228, and the National Natural Science Foundation of China under grant number 51235078. Ting Yu acknowledges the support from the Singapore Ministry of Education under MOE RG199/17S. Cesare Soci acknowledges the support from the Singapore Ministry of Education MOE2011-T3-1-005 and MOE2016-T3-1-006.

ORCID iDs

M Eginligil  <https://orcid.org/0000-0002-4494-7066>

References

- [1] Bonaccorso F, Sun Z, Hasan T and Ferrari A C 2010 Graphene photonics and optoelectronics *Nat. Photonics* **4** 611–22
- [2] Sun Z and Chang H 2014 Graphene and graphene-like two-dimensional materials in photodetection: mechanisms and methodology *ACS Nano* **8** 4133–56
- [3] Yan J, Kim M-H, Elle J A, Sushkov A B, Jenkins G S, Milchberg H M, Fuhrer M S and Drew H D 2012 Dual-gated bilayer graphene hot-electron bolometer *Nat. Nanotechnol.* **7** 472–8
- [4] Bao Q and Loh K P 2012 Graphene photonics, plasmonics, and broadband optoelectronic devices *ACS Nano* **6** 3677–94
- [5] Huang X, Yin Z, Wu S, Qi X, He Q, Zhang Q, Yan Q, Boey F and Zhang H 2011 Graphene-based materials: synthesis, characterization, properties, and applications *Small* **7** 1876–902
- [6] Lee E J H, Balasubramanian K, Weitz R T, Burghard M and Kern K 2008 Contact and edge effects in graphene devices *Nat. Nanotechnol.* **3** 486–90
- [7] Xu X, Gabor N M, Alden J S, Van der Zande A M and McEuen P L 2009 Photo-thermoelectric effect at a graphene interface junction *Nano Lett.* **10** 562–6
- [8] Gabor N M, Song J C W, Ma Q, Nair N L, Taychatanapat T, Watanabe K, Taniguchi T, Levitov L S and Jarillo-Herrero P 2011 Hot carrier-assisted intrinsic photoresponse in graphene *Science* **334** 648–52
- [9] Du X, Skachko I, Barker A and Andrei E Y 2008 Approaching ballistic transport in suspended graphene *Nat. Nanotechnol.* **3** 491–5
- [10] Freitag M, Low T, Xia F and Avouris P 2013 Photoconductivity of biased graphene *Nat. Photonics* **7** 53–9
- [11] Ganichev S and Prettl W 2003 Spin photocurrents in quantum wells *J. Phys. Condens. Matter* **15** R935–83
- [12] Ivchenko E L 2005 *Optical Spectroscopy of Semiconductor Nanostructures* (Harrow: Alpha Science)
- [13] Zhang Y, Tan Y W, Stormer H L and Kim P 2005 Experimental observation of the quantum Hall effect and Berry's phase in graphene *Nature (London)* **438** 201–4

- [14] Castro E V, Novoselov K S, Morozov S V, Peres N M R, Lopes dos Santos J M B, Nilsson J, Guinea F, Geim A K and Castro Neto A H 2007 Biased bilayer graphene: semiconductor with a gap tunable by the electric field effect *Phys. Rev. Lett.* **99** 216802
- [15] McCann E 2006 Asymmetry gap in the electronic band structure of bilayer graphene *Phys. Rev. B* **74** 161403(R)
- [16] Lu G, Yu K, Wen Z and Chen J 2013 Semiconducting graphene: converting graphene from semimetal to semiconductor *Nanoscale* **5** 1353–68
- [17] Ohta T, Bostwick A, Seyller T, Horn K and Rotenberg E 2006 Controlling the electronic structure of bilayer graphene *Science* **313** 951–4
- [18] Wang F, Zhang Y, Tian C, Girit C, Zettl A, Crommie M and Ron Shen Y 2008 Gate-variable optical transitions in graphene *Science* **320** 206–9
- [19] Zhang Y, Tang T T, Girit C, Zhao H, Martin M C, Zettl A, Ron Shen Y and Wang F 2009 Direct observation of a widely tunable bandgap in bilayer graphene *Nature (London)* **459** 820–3
- [20] Taychatanapat T and Jarillo-Herrero P 2011 Electronic transport in dual-gated bilayer graphene at large displacement fields *Phys. Rev. Lett.* **105** 166601
- [21] Park J et al 2011 Single-gate bandgap opening of bilayer graphene by dual molecular doping *Adv. Mater.* **24** 407–11
- [22] Novoselov K S, McCann E, Morozov S V, Fal'ko V I, Katsnelson M I, Zeitler U, Jiang D, Schedin F and Geim A K 2006 Unconventional quantum Hall effect and Berry's phase of 2π in bilayer graphene *Nat. Phys.* **2** 177–80
- [23] Kotov V N, Uchoa B, Pereira V M, Guinea F and Castro Neto A H 2012 Electron–electron interactions in graphene: current status and perspectives *Rev. Mod. Phys.* **84** 1067
- [24] Wang Y, Ni Z, Liu L, Liu Y, Cong C, Yu T, Wang X, Shen D and Shen Z 2010 Stacking-dependent optical conductivity of bilayer graphene *ACS Nano* **4** 4074–80
- [25] Sato K, Park J S, Saito R, Cong C, Yu T, Lui C H, Heinz T F, Dresselhaus G and Dresselhaus M S 2011 Raman spectra of out-of-plane phonons in bilayer graphene *Phys. Rev. B* **84** 035419
- [26] Jiang C, Shalygin V A, Yu Panevin V, Danilov S N, Glaazov M M, Yakimova R, Lara-Avilla S, Kubatkin S and Ganichev S D 2011 Helicity-dependent photocurrents in graphene layers excited by midinfrared radiation of a CO₂ laser *Phys. Rev. B* **84** 125429
- [27] Karch J et al 2010 Dynamic Hall effect driven by circularly polarized light in a graphene layer *Phys. Rev. Lett.* **105** 227402
- [28] Karch J et al 2011 Terahertz radiation driven chiral edge currents in graphene *Phys. Rev. Lett.* **107** 276601
- [29] Olbrich P et al 2013 Reststrahl band-assisted photocurrents in epitaxial graphene layers *Phys. Rev. B* **88** 245425
- [30] Drexler C et al 2013 Magnetic quantum ratchet effect in graphene *Nat. Nanotechnol.* **8** 104–7
- [31] Ganichev S D, Weiss D and Eroms J 2017 Terahertz electric field driven electric currents and ratchet effects in graphene *Ann. Phys.* **529** 1600406
- [32] Kheirabadi N, McCann E and Fal'ko V I 2018 Cyclotron resonance of the magnetic ratchet effect and second harmonic generation in bilayer graphene *Phys. Rev. B* **97** 075415
- [33] Castro Neto A H, Guinea F, Peres N M R, Novoselov K S and Geim A K 2009 The electronic properties of graphene *Rev. Mod. Phys.* **81** 109–62
- [34] Moore J E and Orenstein J 2010 Confinement-induced Berry phase and helicity-dependent photocurrents *Phys. Rev. Lett.* **105** 026805
- [35] Zhu J, Liu Q H and Lin T 2013 Manipulating light absorption in graphene using plasmonic nanoparticles *Nanoscale* **5** 7785–7789
- [36] McIver J, Hsieh D, Steinberg H, Jarillo-Herrero P and Gedik N 2012 Control over topological insulator photocurrents with light polarization *Nat. Nanotechnol.* **7** 96–100